Electronic Supplementary Information

Enhancement of intrinsic thermal conductivity of liquid crystalline epoxy through the strategy of interlocked polymer networks

Sheng Jie Yuan[a], Zhong Quan Peng[b], Min Zhi Rong*[a] and Ming Qiu Zhang*[a]

[a] Key Laboratory for Polymeric Composite and Functional Materials of Ministry of Education, GD HPPC Lab, School of Chemistry, Sun Yat-Sen University, Guangzhou 510275, China

[b] Kingfa Sci. & Tech. Co. Ltd., Guangzhou 510663, China

*Email: cesrmz@mail.sysu.edu.cn (Min Zhi Rong)
*Email: ceszmq@mail.sysu.edu.cn (Ming Qiu Zhang)

Contents of the Electronic Supplementary Information
Number of pages of SI: 21
Number of Figures in SI: 17
Number of Tables in SI: 2

S1. Supplementary Experimental

Synthesis of diglycidyl ether of 4,4'-dihydroxybiphenyl (DGEBP)

According to ref.[S1], diglycidyl ether of 4,4'-dihydroxybiphenyl (DGEBP) was prepared through terminal epoxidation of 4,4'-dihydroxybiphenyl (**Figure S1**), which acted as liquid crystalline epoxy monomer (mesogens) in the present work. Typically, 4,4'-dihydroxybiphenyl (10 g, 0.054 mol), deionized water (9.25 mL), isopropanol (32.875 mL), and epichlorohydrin (42.5 mL, 0.54 mol) were added to a three-point round-bottomed flask equipped with agitator, thermometer, dropping funnel and condensing unit. After being heated to 90 °C, 9.5 mL sodium hydroxide solution (4.65 g NaOH dissolved in 19 mL water) was dropped into the mixture for 1 h, and the reaction proceeded for 1 h. Next, the remaining 9.5 mL sodium hydroxide solution was dropped into the precursor for 1 h and the reaction was continued for 1 h. A large amount of precipitation appeared after finishing the reaction and cooling, which was then filtered and washed with water, 50 vol% ethanol-water solution and ethanol in sequence for three times. White products were obtained and marked by DGEBP. ^{1}H NMR (400 MHz, chloroform-d) δ 7.58 – 7.40 (m, 4H), 7.11 – 6.90 (m, 4H), 4.28 (dd, J = 11.0, 3.2 Hz, 2H), 4.03 (dd, J = 11.0, 5.6 Hz, 2H), 3.40 (ddt, J = 5.7, 4.0, 2.9 Hz, 2H), 2.95 (dd, J = 4.9, 4.1 Hz, 2H), and 2.81 (dd, J = 4.9, 2.7 Hz, 2H).
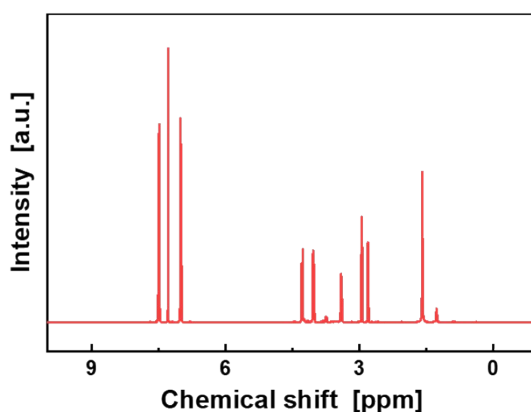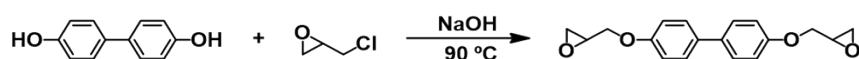

Figure S1. Synthesis and ^{1}H NMR spectrum of DGEBP.

Synthesis of N,N-diglycidyl-furfurlamine (DGFA)

N,N-diglycidyl-furfurlamine (DGFA) was synthesized according to ref.[S2, S3] (**Figure S2**). Epichlorhydrine (20 g, 0.2162 mol) and tetrabutylammonium bromide (5

mol%) were charged into a 500 mL three-necked round-bottom flask. The system temperature was kept at 0 °C, while furfuryl amine (10 g, 0.1031 mol) was added dropwise within 30 min. The reaction proceeded overnight and then 30 mL aqueous sodium hydroxide (40% w/w) was added. The system's temperature was kept at 20 °C under stirring for 12 h. Afterwards, the product was extracted with ethyl acetate and washed with saturated solution of NaCl for three times. The organic layer was collected, dried, and the solvent was removed using a rotary evaporator, leaving an orange liquid. The liquid was further purified using chromatography on a silica gel column with the mixed solvents of ethyl hexane/acetate (3/1). Eventually, a light-yellow liquid was obtained after removal of the solvents under reduced pressure. ^{1}H NMR (400 MHz, DMSO-d_6) δ 7.59 (d, J = 1.8 Hz, 1H), 6.40 (dd, J = 3.1, 1.9 Hz, 1H), 6.32 (t, J = 2.8 Hz, 1H), 3.92 – 3.68 (m, 2H), and 3.10 – 2.32 (m, 10H).
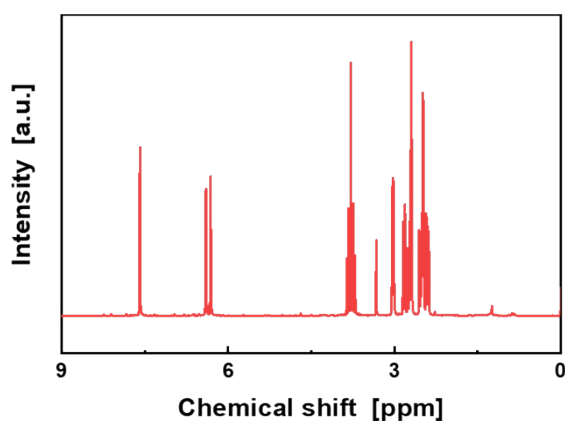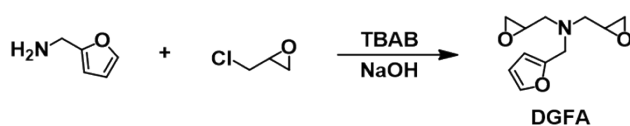

Figure S2. Synthesis and ^{1}H NMR spectrum of DGFA.

R codes used in the orthogonal experiments

```
# Install and import of packages for orthogonal experimental designing.
install.packages("DoE.base")
library(DoE.base)

# Assignment of parameters of orthogonal table, including factors and levels.
# The digit symbols used in 'factor.names' at following code denoting the 5 levels
corresponding to factors have the same meaning as those in Table A.
illce_oa <- oa.design(nfactors = 3, nlevels = c(5, 5, 5), factor.names = list(
                LCE_SchB = c(1, 2, 3, 4, 5), LCE_DA = c(1, 2, 3, 4, 5),
                LCE_SchB_in_ILLCE = c(1, 2, 3, 4, 5)))

# Combination of orthogonal table and results.
TC <- c(...) # The formula and result should be matched.
illce_oa_result <- cbind(illce_oa, TC)

# Intuitive analysis, take factor B as example.
attach(illce_oa_result)
tapply(TC, LCE_DA, mean)
detach(illce_oa_result)

# Variance analysis.
aov.model <-aov(TC ~ as.factor(LCE_SchB) + as.factor(LCE_DA) + as.factor(S_in_ILLCE),
data = illce_oa_result)
summary(aov.model)
```

Figure S3. *R* language codes set used in the orthogonal experiments, including the design of orthogonal table and results analysis.

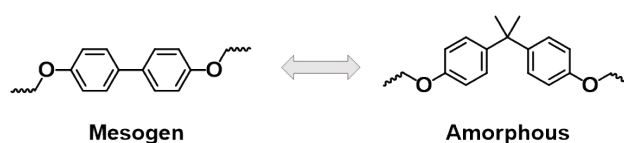### Amorphous control of mesogen used in A-SchB, A-DA and Control-A-*Z*

Figure S4. Structures of the mesogen used in this work and its amorphous control.

Synthesis of L-DA and Control-L-*Z*

The mixture of crosslinked and linear liquid crystalline epoxies (Control-L) were synthesized as follows. DGEBP was modified through epoxy-thiol reaction and end-capped by mono-epoxy monomer containing furfuryl (furfuryl glycidyl ether, FGE), producing the furan-terminated liquid crystalline prepolymer (C-MLCR-S). Then, this prepolymer reacted with BMI to prepare the linear polymer (i.e. linear liquid crystalline

polymer containing DA bonds, L-DA). Finally, LCE-SchB$_{0.500}$ and L-DA were mixed in DMF to obtain Control-L.

FGE was synthesized according to ref.[S4] (**Figure S5**). 51 g (0.55 mol) epichlorohydrin and 3.8 g tetrabutylammonium bromide (TBAB) were charged into a 250 mL three-necked round-bottom flask under argon atmosphere. When the solution was maintained at 25 °C in a water bath, 49 g (0.5 mol) 2-furanemethanol was added dropwise within 30 min. The reaction mixture was stirred for 2 h. After that, 80 mL sodium hydroxide aqueous solution (50% w/v) was added dropwise within 1 h. The reaction proceeded for an additional 4 h at 25 °C. Afterwards, 100 mL ethyl ether was added, and the organic layer was collected, washed with 50 mL saturated solution of NaCl for three times, and dried with anhydrous sodium sulfate, filtrated, and evaporated to get a light-yellow liquid. After distillation of the crude product at 103 - 105 °C in vacuum (11 mmHg), the colorless liquid product was obtained. ^{1}H NMR (400 MHz, DMSO-d_6) δ 7.65 (d, J = 1.4 Hz, 1H), 6.44 (s, 2H), 4.46 (s, 2H), 3.71 (dd, J = 11.5, 2.8 Hz, 1H), 3.33 – 3.23 (m, 1H), 3.09 (ddd, J = 6.6, 4.9, 2.7 Hz, 1H), 2.72 (t, J = 4.7 Hz, 1H), and 2.54 (dd, J = 5.3, 2.7 Hz, 1H).
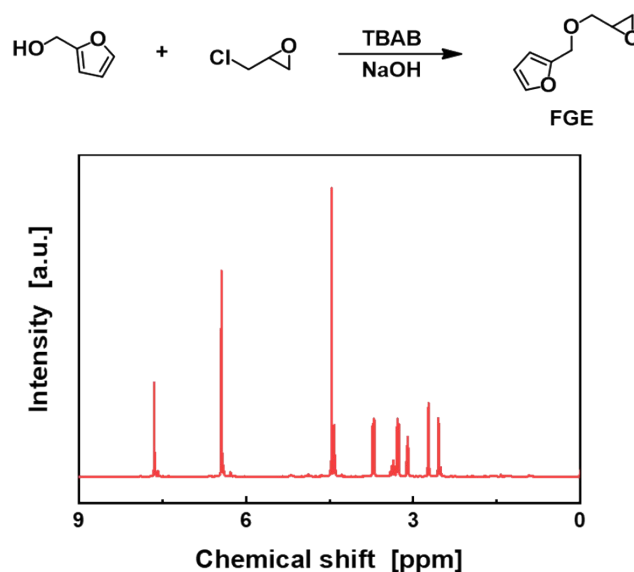

Figure S5. Synthesis and ^{1}H NMR spectrum of FGE.

L-DA was synthesized according to the procedures shown in **Figure S6**. DGEBP (14.9 g, 5×10^{-2} mol), HDTO (12.2 mL, 8×10^{-2} mol) and 100 mL DMF were charged into a three-necked round-bottom flask under argon atmosphere. The reaction was catalyzed by TBD[S5, S6] (5 mol% of epoxy group) at 30 °C for 3 h. Then, FGE (9.24 g, 6×10^{-2} mol) was added and the system was kept on reaction for another 12 h. After

that, the mixture was poured into 25 vol% ethanol aqueous solution to collect the pale yellow prepolymer C-MLCR-S. Finally, the dried C-MLCR-S (15 g) and BMI (1.48 g) were heated to be dissolved in 100 mL DMF at 40 °C, and the as-obtained solution was poured into a mold and dried in vacuum at 80 °C for 2 days to obtained L-DA.
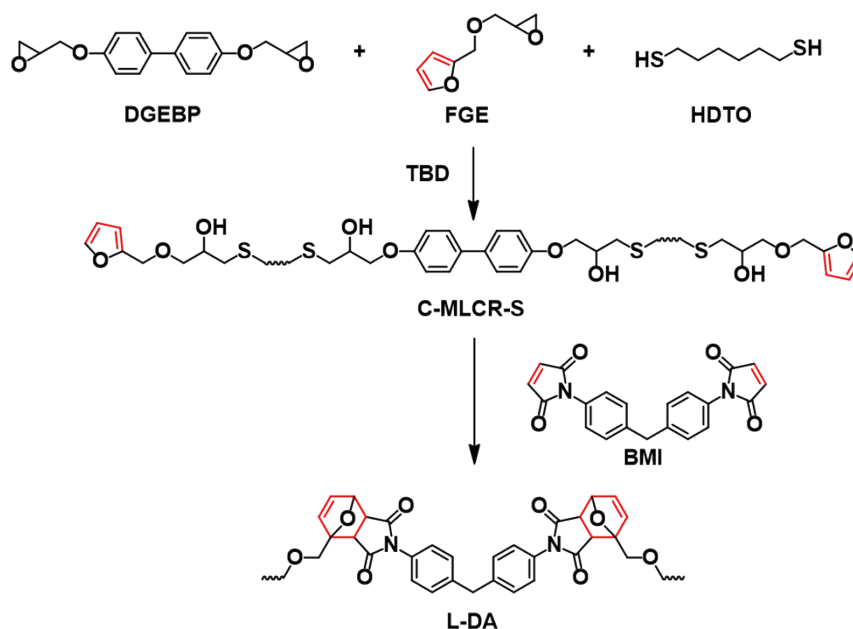

Figure S6. Synthesis of L-DA.

Due to the non-crosslinked structure of L-DA, it could be dissolved in DMF at 80 °C after about 30 min without triggering the DA reaction. Accordingly, after dissolving LCE-SchB$_{0.500}$ (7.5 g) in 150 mL DMF due to Schiff base exchange reaction at 80 °C for 6 h, it was mixed with the as-dissolved L-DA solution (2.5 g in 150 mL DMF). Then, the system was kept on being stirred at 80 °C for 30 min, and concentrated by rotary evaporation. Finally, the solution was poured into a mold and dried in vacuum at 80 °C for 2 days to obtain Control-L-3, where "3" is the mass ratio of LCE-SchB$_{0.500}$ and L-DA.

IPNs-type control

The raw materials of LCE-DA$_{0.6}$ (i.e. MLCR-S and BMI) were firstly dissolved in DMF. Then, the bulk LCE-SchBA$_{0.500}$ was soaked in the solution and swollen for 12 h at room temperature. The IPNs-type control with compositions similar to those of ILLCE$_{0.500/0.6}$-3 was thus produced when the solvent was evaporated.

Synthesis of FPM used in the small molecules model test

The adduct of furan and N-phenylmaleimide (FPM) used for NMR analysis of hydrogen bonding was synthesized according to ref.[S7, S8]. Typically, furan (2.18 mL, 30 mmol) was added to the solution of N-phenyl-maleimide (1.73 g, 10 mmol) in dioxane (30 mL). The reaction was kept at 90 °C for 12 h. Having been cooled down to room temperature, the solvent was removed under reduced pressure, and the residue was dissolved in ethyl acetate. Then, the solutions were poured into excess hexane and stirred intensely. After filtration and drying, the white crystals were obtained. ^{1}H NMR (400 MHz, chloroform-d) δ 7.57 – 7.08 (m, 5H), 6.59 (s, 2H), 5.42 (s, 2H), and 3.04 (d, $J = 1.6$ Hz, 2H).

S2. Supplementary Figures, Tables and Discussion
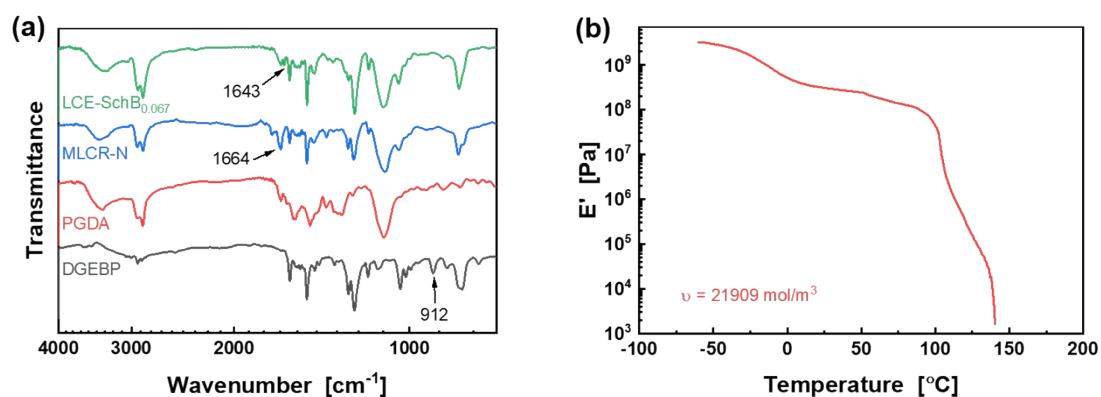
Figure S7. (a) FTIR spectra of the raw materials of MLCR-N and LCE-SchB$_{0.067}$. (b) Temperature-dependence of storage modulus, E', of LCE-SchB$_{0.067}$.
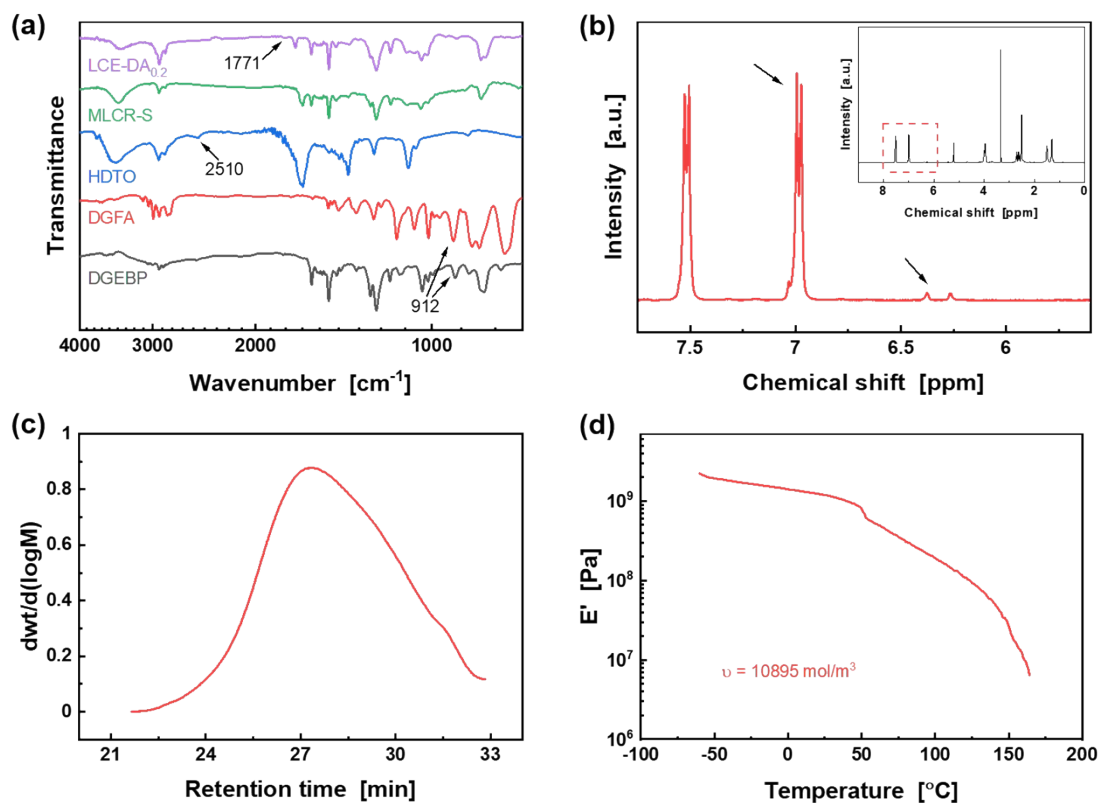

Figure S8. (a) FTIR spectra of the raw materials of MLCR-S and LCE-DA$_{0.2}$. (b) ^{1}H NMR spectrum of MLCR-S. (c) GPC curve of MLCR-S. (d) Temperature-dependence of storage modulus, E', of LCE-DA$_{0.2}$.

The number of furfuryl groups hanging on MLCR-S, n, was estimated from:

$$n = \frac{M_n}{M_{DGEBP} + M_{DGFA} \times y + 150 \times (1 + y)} \times y$$

(S1)

where M_n, M_{DGEBP}, M_{DGFA} and y are the number-average molecular weight determined by GPC, molecular weight of DGEBP, molecular weight of DGFA, and molar ratio of DGFA to DGEBP, respectively.
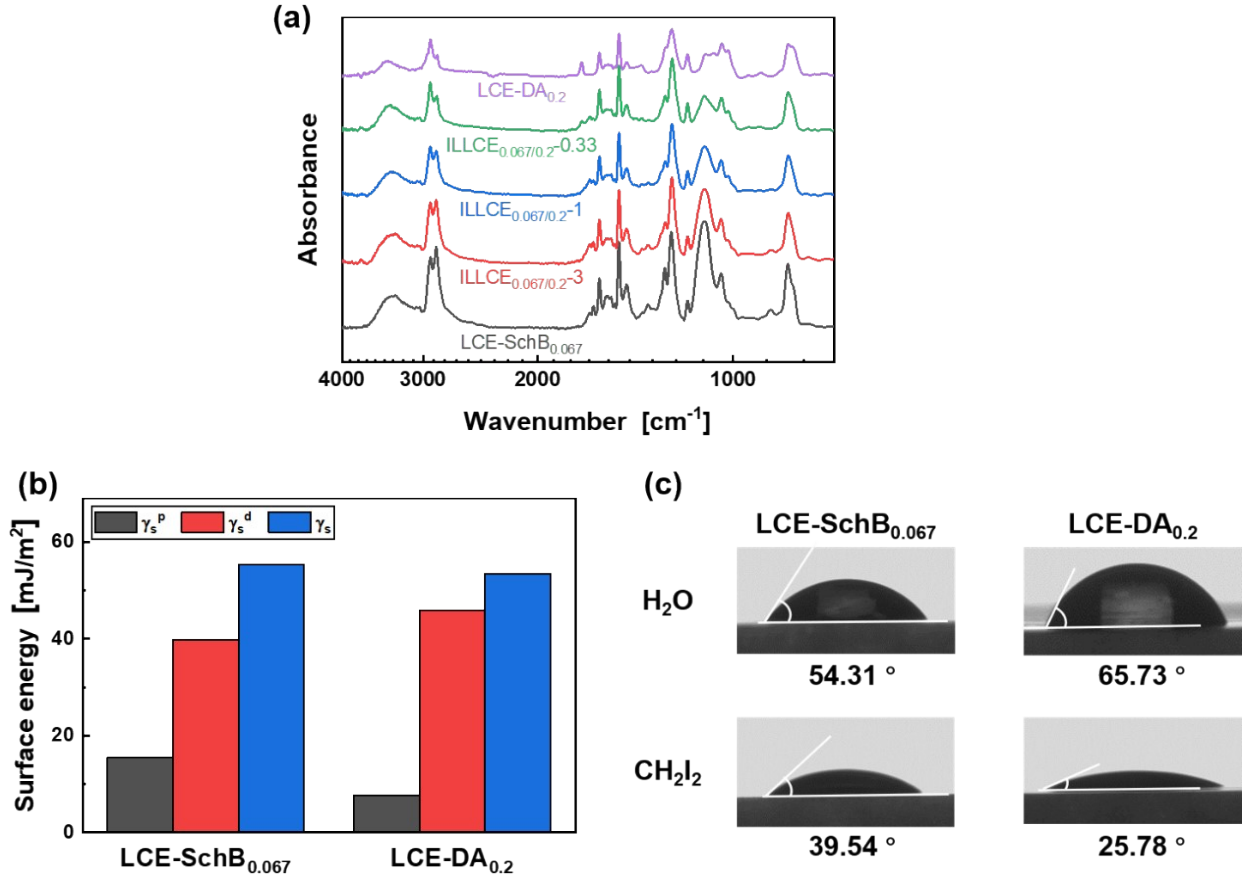
(a)

(b)

(c)

Figure S9. (a) FTIR spectra of $ILLCE_{0.067/0.2}$ with different proportions of the single LCE networks in comparison with those of LCE-SchB$_{0.067}$ and LCE-DA$_{0.2}$. (b) Surface energies and (c) contact angles of LCE-SchB$_{0.067}$ and LCE-DA$_{0.2}$.
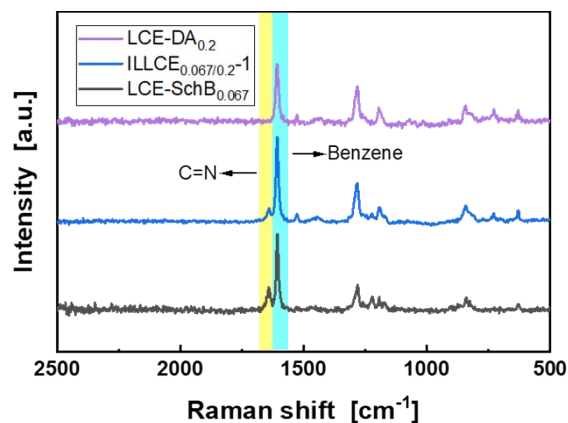
Figure S10. Raman spectra of LCE-SchB$_{0.067}$, LCE-DA$_{0.2}$ and ILLCE$_{0.067/0.2}$-1.
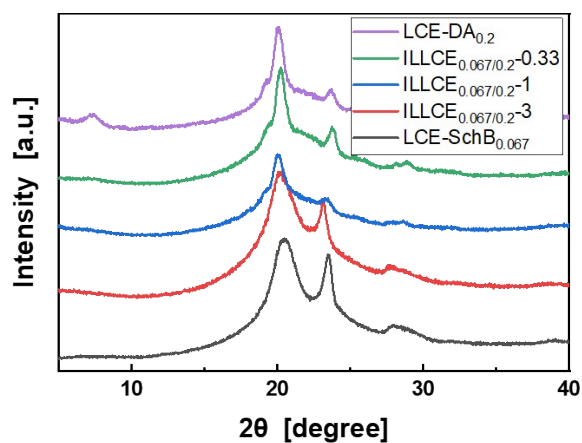

Figure S11. WAXD patterns of LCE-SchB$_{0.067}$, LCE-DA$_{0.2}$ and ILLCE$_{0.067/0.2}$.

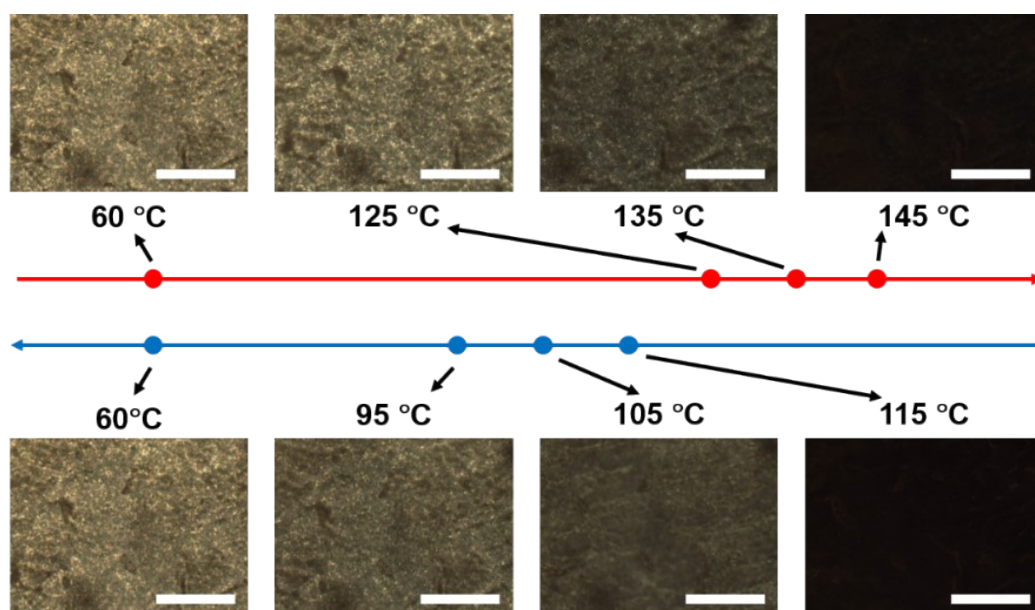**Figure S12**. Temperature-dependent textures of ILLCE$_{0.067/0.2}$-1 observed by POM during heating and cooling. Scale bars: 100 μm.

10

Table S1. Results analysis of the orthographic factorial design (**Table 2**) for enhancing intrinsic thermal conduction of liquid crystalline epoxy in terms of interlocked system

Item		Factor[1]		
		A	B	C
Mean value[2]	K_{i1}	0.2572	0.2654	0.2286
	K_{i2}	0.2522	0.2554	0.2836
	K_{i3}	0.2412	0.2608	0.2738
	K_{i4}	0.2654	0.2550	0.2930
	K_{i5}	0.2608	0.2350	0.1978
Range		0.0242	0.0304	0.0952
S_i[3]		0.00172	0.00314	0.03292
DF_i[4]		4	4	4
MS_i[5]		0.000430	0.000786	0.008229
F_i[6]		0.467	0.854	8.939
$p\ (F_\alpha > F_i)$[7]		0.75870	0.51844	0.00138
$1 - p\ (F_\alpha > F_i)$		0.24130	0.48156	0.99862
Significance		N/A	N/A	Marked

[1]The symbols denoting the three factors have the same meanings as those in **Table 1**.

[2]K_{ij}: Averaged thermal conductivities as a function of factor i and level j.

[3]S_i: Sum of deviation squares of factor i.

[4]DF_i: Degree of freedom of factor i.

[5]MS_i: Mean square of factor i ($MS_i = S_i/DF_i$).

[6]$F_i = MS_i/MS_e$. MS_e represents the mean square of error. In general, the larger F_i, the more significant the influence of the factor on the result.

[7]$p\ (F_\alpha > F_i)$: The probability of the critical value F_α following the F-distribution with degree of freedom (4, 12), in which '4' means the degree of freedom of factor i and '12' means the degree of freedom of error. In this work, F_α is greater than F_i. The smaller $p\ (F_\alpha > F_i)$, the more significant the influence of the factor on the result. The value of $1 - p\ (F_\alpha > F_i)$ represents the confidence coefficient.
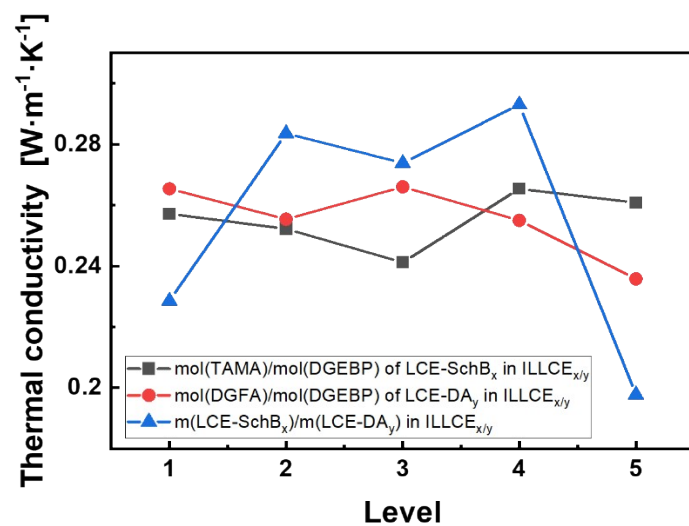
Figure S13. Influence of different levels of the three factors (see **Table 1**) on the averaged thermal conductivities (i.e. the values of K_{ij} listed in **Table S1**).
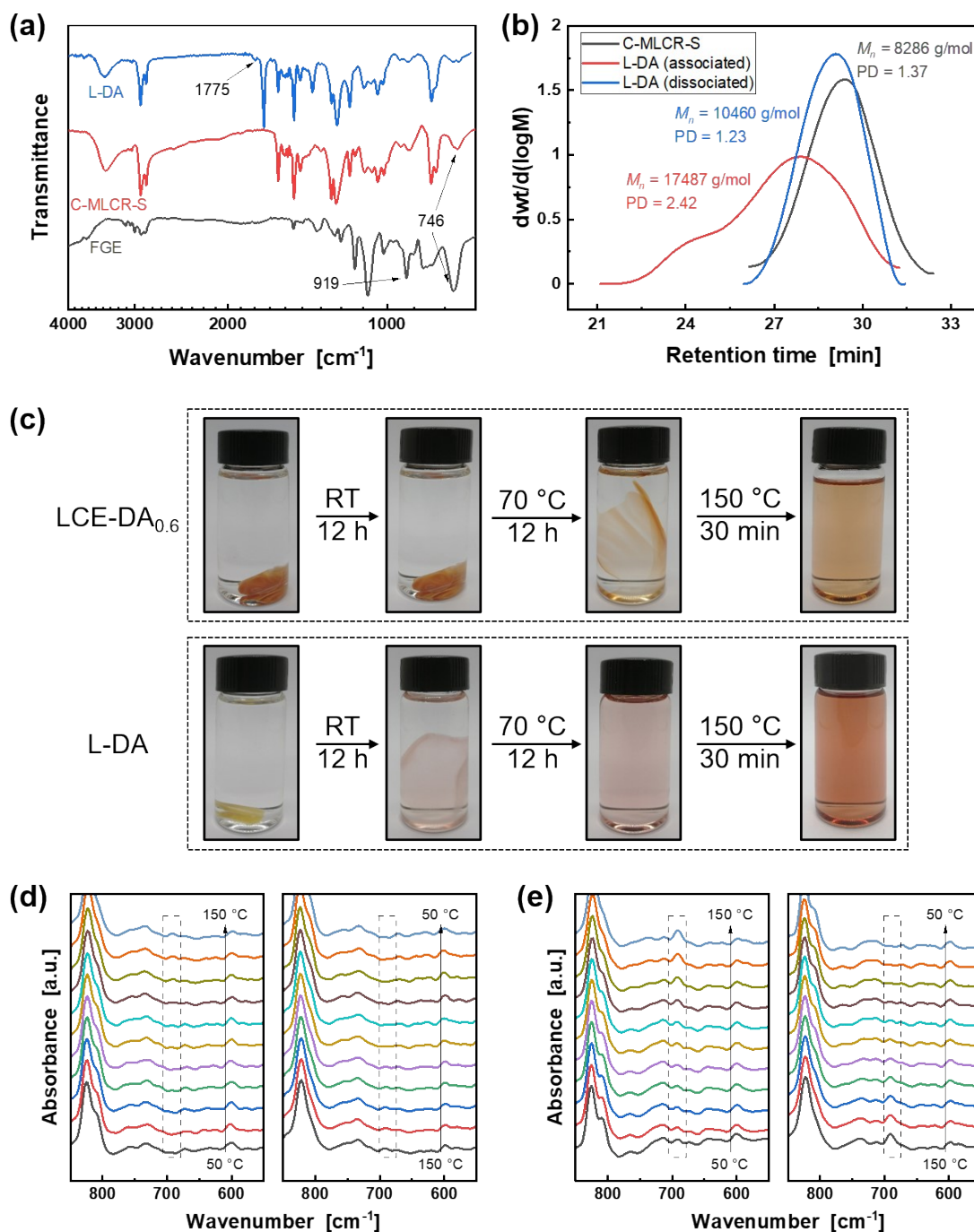
Figure S14. (a) FITR spectra of FGE, C-MLCR-S and L-DA. (b) GPC curves of L-DA in differ states. (c) Swelling and dissolving imagines of L-DA and LCE-DA$_{0.6}$ in DMF. (d, e) Temperature-dependent FTIR spectra of (d) LCE-DA$_{0.6}$ and (e) L-DA.

The linear structure of L-DA was verified as follows. The FTIR spectra in **Figure S14a** indicate that the characteristic peak of epoxy (919 cm^{-1}) was undetectable, but furan ring appears on the spectrum of C-MLCR-S (746 cm^{-1}), meaning successful end capping. Besides, the terminated-furan ring could further react with BMI to obtain L-

DA, so that DA adduct (1775 cm^{-1}) can be detected. Then, swelling experiments of L-DA and LCE-DA$_{0.6}$ were conducted (**Figure S14c**). Having been soaked in DMF at room temperature for 12 h, L-DA and LCE-DA$_{0.6}$ could not be dissolved, but L-DA was greatly expanded while there was not significant change in the size of LCE-DA$_{0.6}$. After that, the soaked samples were heated to 70 °C for 12 h. At this temperature, DA bonds remained stable without breaking, which was testified by the variations of C=C of maleimide with temperature (**Figure S14d** and **Figure S14e**). Consequently, L-DA was completely dissolved in DMF, while LCE-DA$_{0.6}$ was only swollen to bigger size. Without the crosslinked structure, L-DA was more regular than LCE-DA$_{0.6}$. The tighter liquid crystalline regions served as the physical crosslinked points, so that L-DA was insoluble at room temperature, but soluble at 70 °C. As for LCE-DA$_{0.6}$, 70 °C was not high enough to break DA adduct and LCE-DA$_{0.6}$ had to be just swollen. When the samples were further heated to 150 °C for 30 min, LCE-DA$_{0.6}$ became invisible, while the color of the solution of L-DA turned to be darker due to retro-DA reaction. The molecular weights of L-DA at different states were tested (**Figure S14b**). After being dissolved at 70 °C, M_n of the associated L-DA was 17487 g/mol. Besides, after the heat treatment at 150 °C, M_n of the dissociated L-DA decreased to the level of C-MLCR-S.
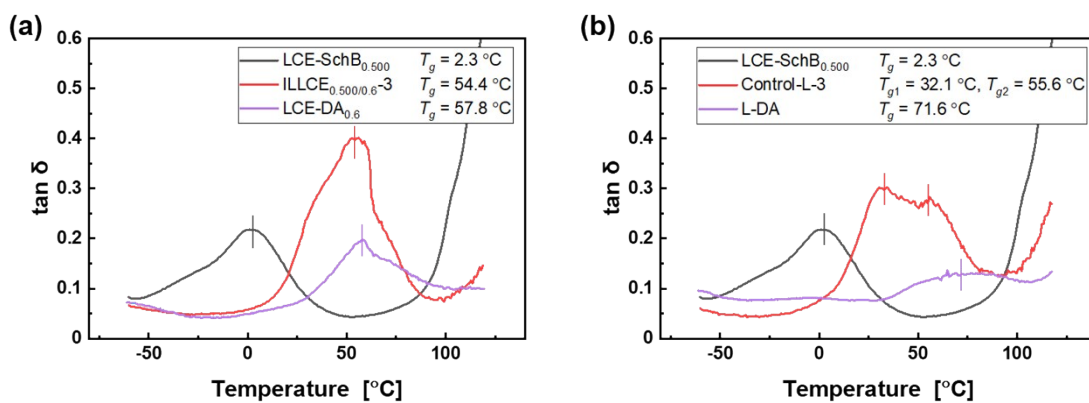

Figure S15. Temperature dependences of loss factor, tan δ, of (a) ILLCE$_{0.500/0.6}$-3 and (b) Control-L-3 in comparison with those of the single networks (heating rate: 3 °C/min; frequency: 1 Hz).
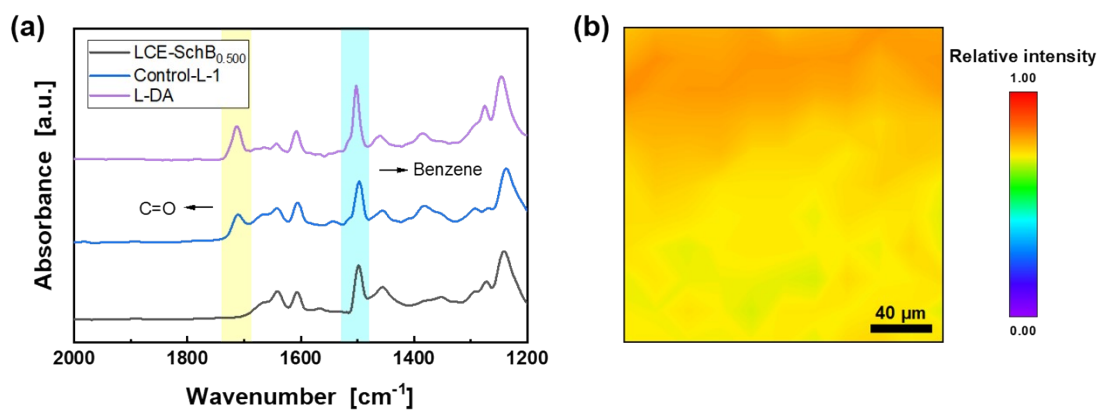
Figure S16. (a) FTIR spectrum of Control-L-1 and (b) micro-infrared spectroscopy analysis of distribution of C=O groups of the DA adducts on the surface of Control-L-1.
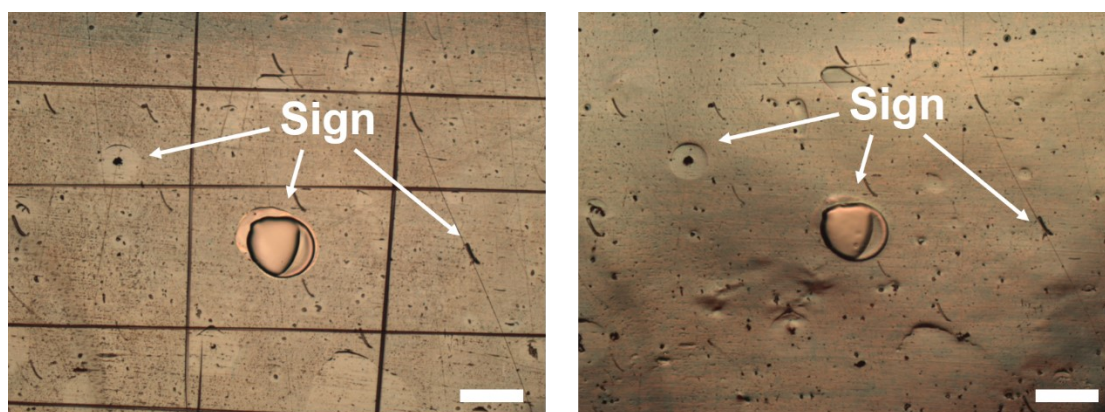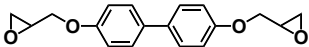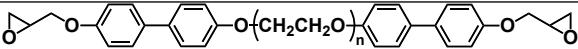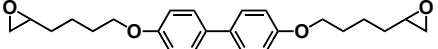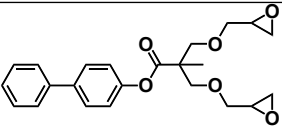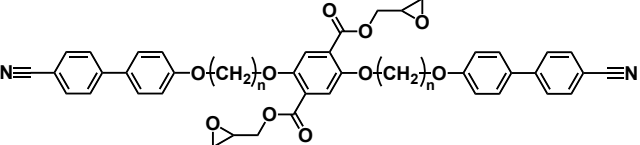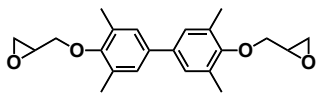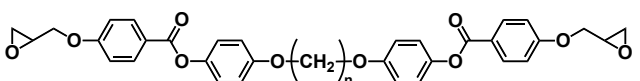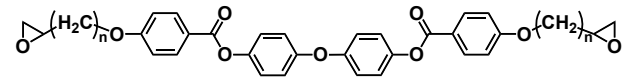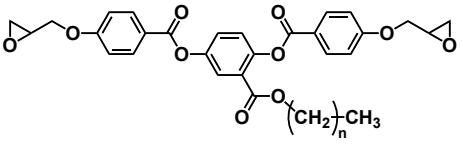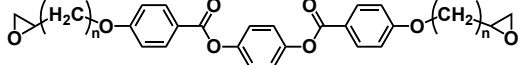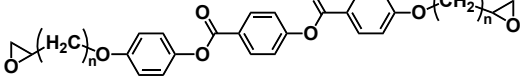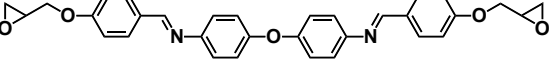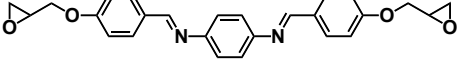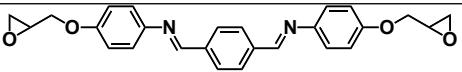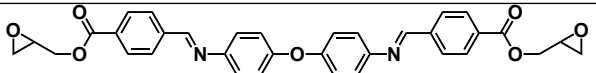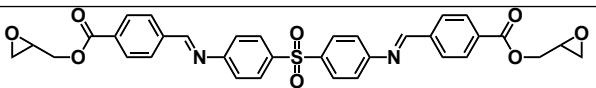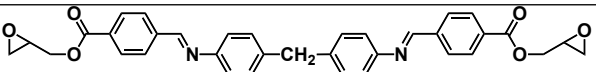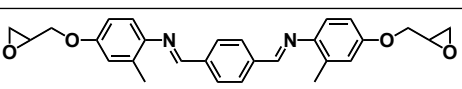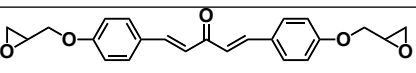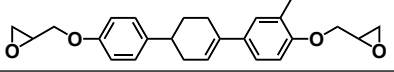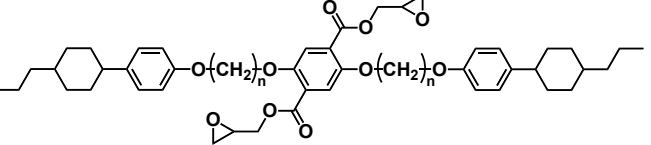

Figure S17. Optical images showing healing effect of the scratched $ILLCE_{0.500/0.6}$-3. Healing condition: 150 °C, 1 h and then 90 °C, 6h. Scale bars: 1 mm.

Table S2. Comparison of thermal conductivities of liquid crystalline epoxies

Epoxy-based mesogen	Content of mesogen, w (wt%)	Thermal conductivity, k (W·m⁻¹·K⁻¹)	k/w (W·m⁻¹·K⁻¹)	Test method	Ref.
	36.81	0.218	0.592	Laser flash	This work (LCE-SchB$_{0.500}$)
	37.27	0.329	0.883	Laser flash	This work (ILLCE$_{0.500/0.6}$-3)
	38.66	0.255	0.66	Laser flash	This work (LCE-DA$_{0.6}$)
	75.06	0.27	0.36	AC calorimetric method	S9
	70.62	0.34	0.481	Hot disk transient plane source (TPS)	S10
	100.00*	0.48	0.480	Hot disk (TPS)	S10
	70.62	0.337	0.477	Hot disk (TPS)	S11
	75.06	0.3	0.400	AC calorimetric method	S12
	85.80	0.51	0.594	Hot disk (TPS)	S13
	79.42	0.31	0.390	Transient hot wire method	S14
	60.43	0.33	0.546	Hot disk (TPS)	S6

Structure	Temp (°C)	Value	Value 2	Method	Ref
	89.16 (n = 6)	0.46	0.516	Hot disk (TPS)	S15
	74.06	0.314	0.424	Hot disk (TPS)	S11
	74.06	0.27	0.365	Laser flash	S16
	86.76	0.33	0.380	Hot disk (TPS)	S17
	87.32 (n = 8)	0.85	0.973	AC calorimetric method	S12
	86.85 (n = 6)	0.89	1.025	AC calorimetric method	S12
	86.34 (n = 4)	0.96	1.112	AC calorimetric method	S12
	81.71 (n =1)	0.292	0.357	Transient hot wire method	S18
	83.73 (n = 4)	0.269	0.321	Transient hot wire method	S18
	76.07 (n = 1)	0.22	0.289	Transient hot wire method	S19
	84.36 (n = 1)	0.25	0.296	Transient hot wire method	S19
	85.63 (n = 5)	0.29	0.339	Transient hot wire method	S19
	86.71 (n = 9)	0.26	0.300	Transient hot wire method	S19
	100.00** (n = 9)	0.31	0.310	Laser flash	S20
	100.00** (n = 9)	0.43	0.430	Laser flash	S20
	80.75	0.30	0.372	Laser flash	S16
	77.54	0.35	0.451	Laser flash	S16

Structure					
(chemical structure: diglycidyl ether bis-Schiff base)	77.54	0.45	0.580	Laser flash	S16
(chemical structure)	82.29	0.35	0.425	Laser flash	S16
(chemical structure with sulfone)	83.42	0.39	0.468	Laser flash	S16
(chemical structure with CH$_2$ bridge)	82.23	0.39	0.474	Laser flash	S16
(chemical structure, methyl-substituted)	89.41	0.38	0.425	Laser flash	S21
	81.14	0.43	0.530	Laser flash	S22
(chemical structure, dienone)	75.30	0.34	0.452	Hot disk (TPS)	S23
(chemical structure)	83.16	0.29	0.349	Laser flash	S24
(chemical structure, n = 4, 8)	94.40 (n = 4, 8)	0.4	0.424	Hot disk (TPS)	S17

*The involved curing reaction followed cationic polymerization initiated by the lab-prepared cationic initiator. Therefore, the content of mesogen was 100 wt%.

**The involved curing reaction followed UV photo-polymerization so that the content of mesogen was 100 wt%.

S3.Reference

(S1) Pei, Z. Q.; Yang, Y.; Chen, Q. M.; Terentjev, E. M.; Wei, Y.; Ji, Y. Mouldable Liquid-Crystalline Elastomer Actuators with Exchangeable Covalent Bonds. *Nat. Mater.* **2014**, *13*, 36-41.

(S2) Dolci, E.; Froidevaux, V.; Michaud, G.; Simon, F.; Auvergne, R.; Fouquay, S.; Caillol, S. Thermoresponsive Crosslinked Isocyanate-Free Polyurethanes by Diels-Alder Polymerization. *J. Appl. Polym. Sci.* **2017**, *134*, 44408.

(S3) Tian, Q.; Yuan, Y. C.; Rong, M. Z.; Zhang, M. Q. A Thermally Remendable Epoxy Resin. *J. Mater. Chem.* **2009**, *19*, 1289-1296.

(S4) Min, Y. Q.; Huang, S. Y.; Wang, Y. X.; Zhang, Z. J.; Du, B. Y.; Zhang, X. H.; Fan, Z. Q. Sonochemical Transformation of Epoxy-Amine Thermoset into Soluble and Reusable Polymers. *Macromolecules* **2015**, *48*, 316-322.

(S5) Yang, X. T.; Guo, Y. Q.; Luo, X.; Zheng, N.; Ma, T. B.; Tan, J. J.; Li, C. M.; Zhang, Q. Y.; Gu, J. W. Self-Healing, Recoverable Epoxy Elastomers and Their Composites with Desirable Thermal Conductivities by Incorporating BN Fillers via in-Situ Polymerization. *Compos. Sci. Technol.* **2018**, *164*, 59-64.

(S6) Yang, X. T.; Zhong, X.; Zhang, J. L.; Gu, J. W. Intrinsic High Thermal Conductive Liquid Crystal Epoxy Film Simultaneously Combining with Excellent Intrinsic Self-Healing Performance. *J. Mater. Sci.* **2021**, *68*, 209-215.

(S7) Utagawa, E.; Sekine, M.; Seio, K. cis-Tetrahydrofuran-3,4-Diol Structure as a Key Skeleton of New Protecting Groups Removable by Self-Cyclization under Oxidative Conditions. *J. Org. Chem.* **2006**, *71*, 7668-7677.

(S8) Yin, G. Y.; Herdtweck, E.; Bach, T. Enantioselective Access to Bicyclo[4.2.0]Octanes by a Sequence of [2+2] Photocycloaddition/Reduction/Fragmentation. *Chem. Eur. J.* **2013**, *19*, 12639-12643.

(S9) Fukushima, K.; Takahashi, H.; Takezawa, Y.; Kawahira, T.; Itoh, M.; Kanai, J. High Thermal Conductive Resin Composites with Controlled Nanostructures for Electric Devices. *IEEJ Trans. FM* **2006**, *126*, 1167-1172.

(S10) Islam, A. M.; Lim, H.; You, N. H.; Ahn, S.; Goh, M.; Hahn, J. R.; Yeo, H.; Jang, S. G. Enhanced Thermal Conductivity of Liquid Crystalline Epoxy Resin Using Controlled Linear Polymerization. *ACS Macro Lett.* **2018**, *7*, 1180-1185.

(S11) Yeo, H.; Islam, A. M.; You, N. H.; Ahn, S.; Goh, M.; Hahn, J. R.; Jang, S. G. Characteristic Correlation between Liquid Crystalline Epoxy and Alumina Filler on Thermal Conducting Properties. *Compos. Sci. Technol.* **2017**, *141*, 99-105.

(S12) Akatsuka, M.; Takezawa, Y. Study of High Thermal Conductive Epoxy Resins Containing Controlled High-Order Structures. *J. Appl. Polym. Sci.* **2003**, *89*, 2464-2467.

(S13) Yang, X. T.; Zhu, J. H.; Yang, D.; Zhang, J. L.; Guo, Y. Q.; Zhong, X.; Kong, J.; Gu, J. W. High-Efficiency Improvement of Thermal Conductivities for Epoxy Composites from Synthesized Liquid Crystal Epoxy Followed by Doping BN Fillers. *Compos. Part B-Eng.* **2020**, *185*, 107784.

(S14) Zhang, Q.; Chen, G. K.; Wu, K.; Shi, J.; Liang, L. Y.; Lu, M. G. Biphenyl Liquid Crystal Epoxy Containing Flexible Chain: Synthesis and Thermal Properties. *J. Appl. Polym. Sci.* **2020**, *137*, 49143.

(S15) Jeong, I.; Kim, C. B.; Kang, D. G.; Jeong, K. U.; Jang, S. G.; You, N. H.; Ahn, S.; Lee, D. S.; Goh, M. Liquid Crystalline Epoxy Resin with Improved Thermal Conductivity by Intermolecular Dipole-Dipole Interactions. *J. Polym. Sci., Part A: Polym. Chem.* **2019**, *57*, 708-715.

(S16) Giang, T.; Kim, J. Effect of Liquid-Crystalline Epoxy Backbone Structure on Thermal Conductivity of Epoxy-Alumina Composites. *J. Electron. Mater.* **2016**, *46*, 627-636.

(S17) Kim, Y.; Yeo, H.; You, N. H.; Jang, S. G.; Ahn, S.; Jeong, K. U.; Lee, S. H.; Goh, M. Highly Thermal Conductive Resins Formed from Wide-Temperature-Range Eutectic Mixtures of Liquid Crystalline Epoxies Bearing Diglycidyl Moieties at the Side Positions. *Polym Chem.* **2017**, *8*, 2806-2814.

(S18) Chen, G. K.; Zhang, Q.; Hu, Z. R.; Wang, S.; Wu, K.; Shi, J.; Liang, L. Y.; Lu, M. G. Liquid Crystalline Epoxies Bearing Biphenyl Ether and Aromatic Ester Mesogenic Units: Synthesis and Thermal Properties. *J. Macromol. Sci. A* **2019**, *56*, 484-495.

(S19) Guo, H. L.; Lu, M. G.; Liang, L. Y.; Wu, K.; Ma, D.; Xue, W. Liquid Crystalline Epoxies with Lateral Substituents Showing a Low Dielectric Constant and High Thermal Conductivity. *J. Electron. Mater.* **2016**, *46*, 982-991.

(S20) Tokushige, N.; Mihara, T.; Koide, N. Thermal Properties and Photo-Polymerization of Diepoxy Monomers with Mesogenic Group. *Mol. Cryst. Liq. Cryst.* **2006**, *428*, 33-47.

(S21) Harada, M.; Hamaura, N.; Ochi, M.; Agari, Y. Thermal Conductivity of Liquid Crystalline Epoxy/BN Filler Composites Having Ordered Network Structure. *Compos. B. Eng.* **2013**, *55*, 306-313.

(S22) Harada, M.; Ochi, M.; Tobita, M.; Kimura, T.; Ishigaki, T.; Shimoyama, N.; Aoki, H. Thermal-Conductivity Properties of Liquid-Crystalline Epoxy Resin Cured under a Magnetic Field. *J. Polym. Sci., Part B: Polym. Phys.* **2003**, *41*, 1739-1743.

(S23) Lin, Y. S.; Hsu, S. L. C.; Ho, T. H.; Cheng, S. S.; Hsiao, Y. H. Synthesis, Characterization, and Thermomechanical Properties of Liquid Crystalline Epoxy Resin Containing Ketone Mesogen. *Polym. Eng. Sci.* **2017**, *57*, 424-431.

(S24) Tanaka, S.; Hojo, F.; Takezawa, Y.; Kanie, K.; Muramatsu, A. Formation of Liquid Crystalline Order and Its Effect on Thermal Conductivity of AlN/Liquid Crystalline Epoxy Composite. *Polym. Plast. Technol. Eng.* **2017**, *57*, 269-275.